Biochemical and Biological Characterization of KRAS Q61 Mutants

By: Adelaide Cooke

Senior Honors Thesis
Department of Biology
University of North Carolina at Chapel Hill

5 December 2018

Approved:

Dr. Channing Der, Thesis Advisor

Dr. Steve Matson, Reader 1

Dr. Scott Williams, Reader 2

Abstract

Nearly 30% of human cancers have mutations in one of the three RAS genes. Despite over 30 years of dedicated research, no effective therapies against cancers caused by RAS oncogene mutations have reached clinical application. Striking differences in the frequencies of missense mutations seen in RAS-mutant cancers suggest that RAS mutations previously assumed to equally result in activation have distinct consequences on protein structure and function. We hypothesized that different point mutations at the hotspot residue Q61 will have distinct consequences on RAS structure and function, resulting in unique biological activities. We evaluated the effects on biochemical and biological properties of the common mutants KRAS Q61H, KRAS Q61L, and KRAS Q61R and the rare KRAS Q61E and KRAS Q61P. We found that these KRAS Q61 mutants exhibited varying trends of guanine nucleotide exchange as well as binding to RAS effector domains in vitro. KRAS Q61L exhibited increased GEF-stimulated nucleotide exchange, whereas the Q61R and Q61P mutants were poorly responsive to GEFs. Ectopic expression of KRAS Q61 mutants in NIH 3T3 and RIE-1 cells revealed variable mutation-dependent effector signal activation, morphologic transformation and anchorage-independent growth. Unlike the other mutants, KRAS Q61E and KRAS Q61P did not appear to be activated based on morphological traits. Analysis of signaling through RAS effectors indicated these mutants were still activated; however, it still suggested that they are biologically different from each other. Q61 mutants do not equally induce actin stress fiber formation, cell migration and KRAS-dependent macropinocytosis. Our studies suggest that determination of RAS mutation-specific effects will allow for identification of mutation-selective vulnerabilities and therapies for KRAS Q61 mutants.

Introduction

Mutations to RAS genes are associated with major causes of cancer deaths and are found in approximately 30% of all human cancers [1-3]. As of 2017, the three cancers with the highest percentage of deaths in the United States were lung and bronchus, colon and rectum, and pancreatic cancers [4-5]. Combined, these cancers resulted in over 40% of the total estimated cancer deaths in the United States [6]. Unsurprisingly, these cancers have some of the lowest 5-year survival rates; pancreatic cancer has the lowest with only an 8% 5-year survival rate [7]. The frequency of RAS mutation in each of these cancers is very high, indicating the importance of studying RAS proteins to develop novel cancer treatments. In fact, the majority of pancreatic ductal adenocarcinoma (PDAC) tumors are driven by constitutive activation of the GTPase KRAS [8-10]. However, despite more than 30 years of dedicated research, there has been no effective "anti-RAS" therapy to reach clinical application [4-5].

The three RAS genes (HRAS, KRAS, and NRAS) encode four closely related proteins (HRAS, KRAS4A and KRAS4B splice variants, and NRAS) [11]. HRAS and NRAS each have one protein product. KRAS4B and KRAS4A are splice variants of the KRAS gene product which differ in their carboxyl terminal hypervariable region; KRAS4A contains exon 4A, whereas KRAS4B contains alternative exon 4B [11-12]. These four RAS proteins are very similar, owing to 80-90% overall sequence homology among the RAS isoforms [3, 13-14]. The most significant divergence in homology between the RAS isoforms occurs at the C-terminal hypervariable region of each protein [16, 27-28]. It has been speculated that the isoform-specific actions result from membrane localization differences due to the variation at the C-terminus [14, 29-30].

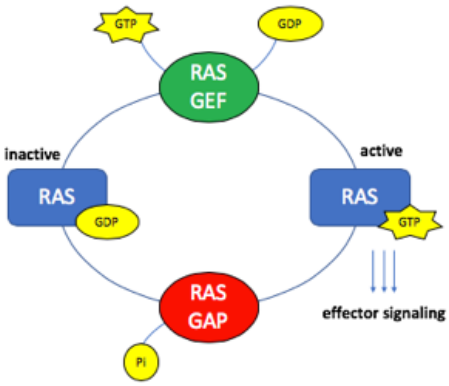

Figure 1. The GTPase Cycle of RAS

The RAS proteins are predominantly membrane-localized [5, 15-18]. Functionally, RAS proteins are small GTPases that serve as molecular switches that cycle between a GTP-bound "active" state and a GDP-bound "inactive" state (Figure 1) [19-21]. While RAS is capable of cycling independently, the presence of guanine nucleotide exchange factors (GEFs) and GTPase-activating proteins (GAPs) speed up these processes significantly [19, 22-23]. GEFs promote the nucleotide exchange of GDP for GTP leading to activation of the RAS proteins [21]. GAPs stimulate the hydrolysis of GTP leading to inactivation [21, 24]. Once GTP-bound, RAS can go on to regulate many signaling pathways governing cell proliferation, differentiation, and survival (Figure 3) [3, 13-14]. Aberrant RAS function is associated with constitutive activation, leading to variation in pathway regulation [13, 22] This results in increased cell proliferation, growth, and survival, which are hallmark characteristics of cancer [25].

While there are over 130 different missense RAS mutations found in cancer, the predominant "hotspot" mutations occur at codons G12, G13, and Q61. [26-27] Mutations at these hotspot locations impair GTP hydrolysis and/or promote nucleotide exchange rates, resulting in abnormal activation of RAS which leads to uncontrolled cellular growth and proliferation [27]. Due to the focus on a subset of HRAS mutations in early

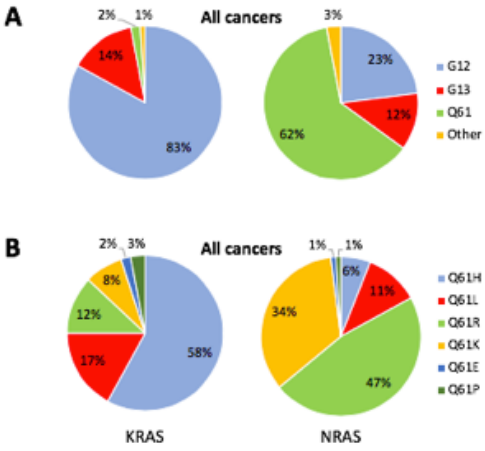

Figure 2. RAS mutations in cancer. A. KRAS is predominantly mutated at G12; NRAS is predominantly mutated at Q61. **B.** The frequency of specific missense mutations at Q61 are strongly different between KRAS and NRAS. Compiled from COSMIC.

studies on RAS biology (HRAS G12V, G12D), all mutations to these hotspots were assumed to be "universally" activating and equally potent in driving oncogenic growth [27]. While informative, these prior studies were largely unsuccessful in producing anti-RAS therapies, in part due to the assumption that not only were all RAS proteins were identical in function, but that all mutations to RAS resulted in identical structural and biochemical perturbations [1, 13, 20].

One piece of evidence that suggests RAS mutations do not cause equivalent changes in function is the discrepancy in mutation frequency between the RAS isoforms. In cancer, KRAS is the most commonly mutated, followed by NRAS and then HRAS [5, 31]. Prevalence of mutations in each isoform also vary depending on the cancer. For example, KRAS mutations are most frequent in pancreatic and colon cancers while NRAS mutations are predominantly found in lymphoid cancers and melanomas [2, 5, 28]. The frequency of mutations at the hotspot residues also vary greatly between the RAS genes. KRAS mutations occur predominantly at G12 (83%); in contrast, NRAS is preferentially mutated at Q61 (62%) (Figure 2A) [31]. Moreover, specific missense mutations do not occur at equivalent frequencies between RAS isoforms: looking at Q61, the most common mutations in KRAS and NRAS are Q61H and Q61R respectively (Figure 2B) [31]. Together, these differences suggest that a mutation-specific approach may be required for successful anti-RAS therapies.

RAS participation in cellular signaling pathways contributes to oncogenic growth by controlling cellular proliferation, differentiation, and survival. [3, 13, 14, 32] There are four canonical RAS signaling pathways implicated in cancer: ERK1/2-MAPK, PI3K-AKT, TIAM1-RAC, and RALGEF-RAL (Figure 3) [4]. For many of our studies, we focused on the ERK1/2-MAPK and PI3K-AKT pathways due to their widespread activation in cancer. In the MAPK pathway, activated RAS

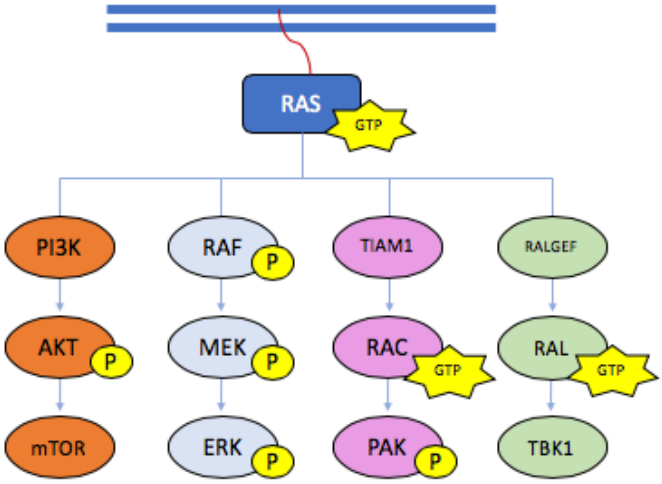

Figure 3. RAS-mediated effector signaling pathways

binds to RAF. Once activated, RAF phosphorylates MEK1/2, which in turn activates ERK1/2 via phosphorylation. This signaling cascade leads to cellular growth signaling and cell cycle progression; when constitutively active, this results in aberrant growth [33-35]. In the PI3K-AKT pathway, activated RAS initially binds to PI3K. This binding event leads to the phosphorylation of AKT, which in turn phosphorylates mTOR resulting in activation of further downstream signaling nodes promoting cell survival [4]. Additionally, RAS activation does not strictly result in linear signaling pathways due to complex communication pathways and feedback loops across RAS-mediated signaling nodes, contributing to its "undruggable" nature [13, 20, 27].

Our research focused on the RAS mutation hotspot Q61. Q61 is located in the Switch 2 region of RAS, which is required for the binding of GTP and engagement of several downstream effector proteins. The Q61 residues also resides near the GAP binding site and is responsible for coordinating the catalytic water molecule used for GTP hydrolysis [35-36]. Therefore, it is believed that mutations at Q61 disrupt intrinsic and GAP-mediated hydrolysis, rendering the mutated protein constitutively active [37]. However, RAS activation is not solely dependent on the population of the activated GTP-bound state, as changes in membrane localization or protein structural changes may also play a role in altering effector signaling [35, 37].

Given that there has not been substantial research on individual RAS Q61 mutations, we wanted to determine the biological and functional differences among Q61 mutants in RAS. For our studies, we focused our experiments on five KRAS Q61 mutations (Q61H, Q61L, Q61R, Q61E, and Q61P) that result from single-base substitutions. These Q61 mutations occur at strikingly inequivalent frequencies among the RAS isoforms [31]. The Q61H and Q61R mutations show RAS isoform-specific frequencies as previously mentioned, whereas Q61L occurs at a similar frequency across all RAS isoforms. Interestingly, the Q61E and Q61P mutations are rare in all RAS-mutant cancers (Figure 2B). Due to the numerous background mutations found in cancer cell lines, we first investigated mutation-specific effects in model systems with clean genetic backgrounds (NIH 3T3s, RIE-1s). To characterize these mutations, we utilized western blotting analysis, confocal microscopy and immunofluorescence-based assays using KRAS Q61 mutants to determine basic biological and functional differences. Additional biochemical assays, including nucleotide exchange and effector binding, were performed to further characterize functional differences among the mutants.

Methods

Cell Culture

Human embryonic kidney cells (HEK 293T) and rat intestinal epithelial cells (RIE-1) were maintained in Dulbecco's Modified Eagle Medium (DMEM) supplemented with 10% fetal bovine serum (FBS) and penicillin/streptomycin. Mouse embryonic fibroblast cells (NIH 3T3) were maintained in DMEM supplemented with 10% Colorado Calf Serum (CCS) and penicillin/streptomycin.

Mutant KRAS DNA was cloned into a retroviral mammalian expression vector (pBABE-puro). Retrovirus was produced in HEK-293T cells via transfection of the pBABE-puro target vector and a pCL-10A1 packaging vector. Transfected HEK-293T cells were allowed to produce retrovirus for 24 hr. Retrovirus was then harvested and placed on target cells in the presence of 2 μg/mL polybrene. Cells were incubated with retrovirus for 8 hr. Fresh media was then added and antibiotic selection was applied 24 hr later (2 μg/mL puromycin).

Experimental Controls

EV was used as the empty vector control to show the successful infection of our experimental samples with KRAS DNA. KRAS WT served as a negative control since the wild type protein exhibits normal biochemical and biological phenotypes and functions. KRAS G12D served as a positive control in some experiments since it is the one of the most common occurring (and one of the most studied) oncogenic RAS mutations.

Light Microscopy Analysis

NIH 3T3 mouse embryonic fibroblasts were stably infected with mutant KRAS DNA and plated on plastic dishes. Light microscopy images were taken 72 hours after antibiotic selection. Images were taken at 10X magnification on a Nikon Eclipse T5100 light microscope. This was repeated in RIE-1 cells. (n=3)

Soft Agar Growth Analysis

NIH 3T3 mouse embryonic fibroblasts were stably infected with mutant KRAS DNA. They were plated in soft agar. After 5 days, cells were imaged, and colonies were quantified after labeling with Calcein AM cell viability dye using a SpectraMax MiniMax. This was repeated in RIE-

1 cells. Statistical analysis was performed using a two tailed T test on PRISM software. Error bars indicated standard error.

Determining Cell Signaling using Western Blotting

Cell lysates were harvested from the mutant KRAS-infected cells (RIE-1 and NIH 3T3) and normalized for total protein concentration using a Bio-Rad assay. Lysates were then run on an SDS-PAGE gel at 60 V for 10 min to ensure equal loading and then at 150 V for 1 hr. Lysates were then transferred to a PVDF membrane for 90 min at 90 V. The membranes were blocked in 5 % milk for 1 h and then incubated with primary antibodies overnight at 4°C. Primary antibodies used were anti-HA (Covance MMS-101P-200); anti-vinculin (Sigma #V9131); anti-actin (Sigma #A541); phospho-MEK1/2 (Cell Signaling #9154S); anti-MEK1/2 (Cell Signaling #46945); phospho-ERK1/2 (Cell Signaling #4370); anti-ERK1/2 (Cell Signaling #9201); phospho-AKT (Cell Signaling #9271S); and anti-AKT (Cell Signaling #9272). Membranes were washed three times with Tris buffered saline with Tween (TBS-T). The membranes were incubated with secondary antibodies for 1 hr and washed three times with TBS-T. Chemiluminescent reagent was then added and proteins were visualized on a Bio-Rad ChemiDoc Imaging system. (n>3)

Macropinocytosis Assays

RIE-1 cells stably expressing mutant KRAS were used for performing macropinocytosis assays. The cells were serum-starved overnight. In the morning, the media was changed and a fluorescent sugar, FITC-dextran, was added to the cells (1:1000) for 30 minutes. Cells were then washed with PBS and fixed for imaging. Nuclei were stained using DAPI. The cell samples were imaged on a Zeiss LSM 700 confocal microscope. Statistical analysis was performed using a two tailed T test on PRISM software. Error bars indicated standard error. Three asterisks designate

the most significantly different observations, followed by two asterisks designating the second most significantly different observations. All remaining data is statistically significant; however, they have no asterisk designation. (n=3)

Stress Fiber Formation Assays

NIH 3T3 cells stably expressing mutant KRAS were used for imaging actin stress fiber formation. Cells were plated onto glass slides coated with fibronectin, and the cells were fixed with formaldehyde. The cells were then permeabilized to allow for antibody staining. After the cells were blocked, they were incubated with phalloidin (for F-actin staining, Alexa Fluor 488 Phalloidin) or anti-vinculin antibody (1:200) for 60 min at room temperature. After washing the primary antibodies off, the cells were incubated with Alexa-Fluor secondary antibody (1:200) for 45 min at room temperature. The slides were then mounted onto glass coverslips for immunofluorescence imaging. Stained cells were imaged on a Zeiss LSM 700 confocal microscope. Statistical analysis was performed using a two tailed T test on PRISM software. Error bars indicated standard error. Three asterisks designate the most significantly different observations, followed by two asterisks designating the second most significantly different observations. All remaining data is statistically significant; however, they have no asterisk designation. (n=3)

Cell Migration Assays

NIH 3T3 cells stably expressing mutant KRAS were used for random cell migration assays. Cells were plated at less than confluent densities onto 35 mm glass Mattek dishes coated with fibronectin. The dishes were then imaged on an Olympus VivaView Incubator Microscope at a 10X objective. Cells were then imaged for 12-16 hours in order to track cell migration. Collected

images were combined into migration videos to allow for individual cell tracking. The average distance and velocity of each KRAS mutation was quantified based on the average of > 60 individual cells per condition. Statistical analysis was performed using a two tailed T test on PRISM software. Error bars indicated standard error. (n=3, N>60 cells per KRAS mutation)

Protein Expression and Purification

Protein expression vectors for KRAS WT, subsequent KRAS mutants, the RAS GEF SOS (catalytic domains), and effector domain proteins were generated previously. All proteins were expressed in E. coli cells with corresponding antibiotics and harvested for protein purification. Cells were pelleted and lysed using sonication. The protein lysate was pelleted, and the supernatant was added to a nickel column. After a series of washes, the protein was eluted off of the column in a buffer containing high imidazole (300 mM). TEV protease, an enzyme that cleaves off the nickel purification tag, and 1 mmol reducing agent were added to the protein and left to dialyze overnight. Any uncleaved protein was removed by a second column purification after overnight dialysis. Protein purity was confirmed by SDS-PAGE analysis.

RAS Nucleotide Exchange Assays

Purified KRAS protein was loaded with a fluorescent nucleotide analog (mant-GTPγS). The protein was buffer exchanged away from excess magnesium and incubated with 5-fold excess of nucleotide overnight. The following day, 60 µmol magnesium was added to facilitate nucleotide binding. The samples were loaded onto a size exclusion column, and fractions were collected. The fractions with the most protein were pooled and kept on ice. The protein concentration was determined using a protein A280 assay. Nucleotide exchange assays were performed on an Agilent Cary Eclipse Fluorescence Spectrophotometer. Nucleotide-loaded KRAS was added to 1

μM in 1 mL of exchange buffer in the presence and absence of SOS. Unlabeled GDP was added in excess (1:1000) next to initiate the exchange reaction, and the change in fluorescence was monitored for the duration of the assay. EDTA was added at the very end to chelate the magnesium and end the exchange assay. Statistical analysis was performed using a two tailed T test on PRISM software. Error bars indicated standard error. Three asterisks designate the most significantly different observations, followed by two asterisks designating the second most significantly different observations. All remaining data is statistically significant; however, they have no asterisk designation. (n=3)

Effector Binding Assays

KRAS protein and effector fragments were purified using the same methods used for nucleotide exchange. The purified KRAS proteins were loaded with the non-hydrolyzable nucleotide mant-GMPPNP. Effector binding assays were performed on a SpectraMax M5 plate reader. Nucleotide-loaded KRAS was incubated with different concentrations of effector proteins. Nucleotide exchange was then stimulated with the addition of excess GDP (1:1000) and the change in fluorescence was monitored. The changes in rates of nucleotide exchange were plotted against effector protein concentrations to determine binding affinity. Statistical analysis was performed using a two tailed T test on PRISM software. Error bars indicated standard error.

Results

Our studies focused on biochemically and biologically studying KRAS Q61 mutations. We expected that the mutations would be different in these aspects based on literature referencing RAS sequence homology, RAS isoform prevalence, mutation prevalence among and between RAS isoforms, and previous functional studies.

Light Microscopy Analysis

Light microscopy was used to take images of NIH 3T3 mouse embryonic fibroblasts infected with KRAS Q61 mutants growing on plastic. In this classical model cell line, KRAS-transformed cells become highly refractile more rounded and more "spindle-like" as shown by the KRAS G12D-transformed cells, which serve as a known activated KRAS control (Figure 4). Most of the KRAS Q61-transformed cells also exhibited similar phenotypes (Q61H, Q61L, Q61R). However, KRAS Q61E and Q61P-transformed cells did not exhibit the same changes in cellular morphology. Visibly, these KRAS-mutant lines more closely resembled the KRAS wild-type and empty vector control cell lines. This was repeated in RIE-1 cells with similar results.

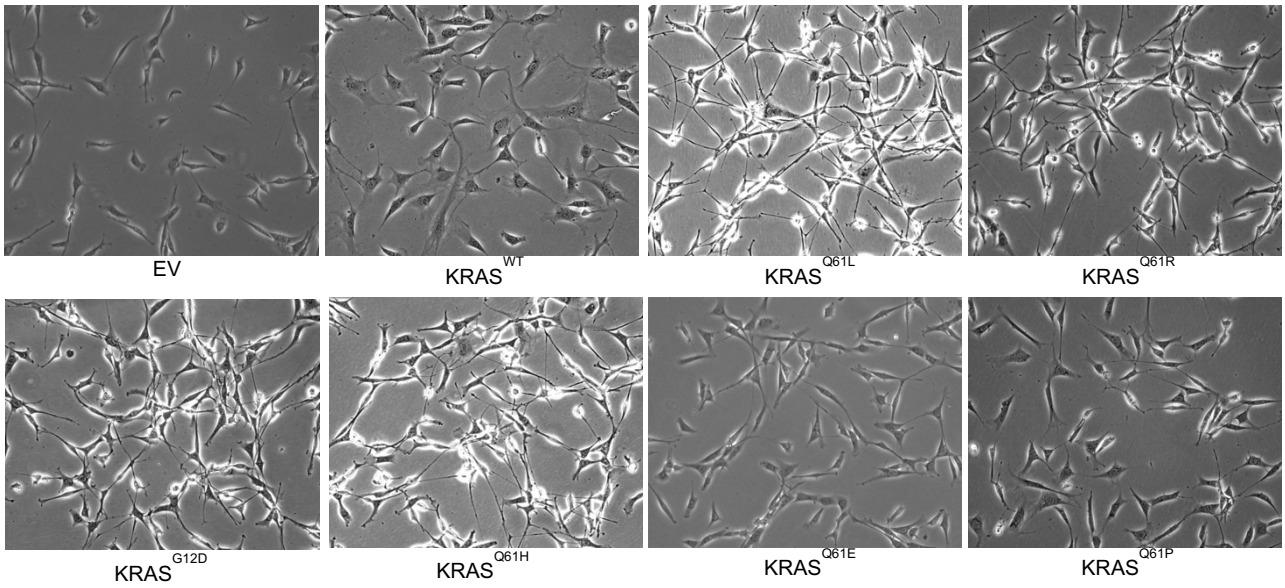

Figure 4. KRAS Q61 mutations do not cause equivalent transformation in cell morphology. NIH 3T3 mouse embryonic fibroblasts were stably infected with mutant KRAS DNA. Images were taken at 10X magnification on a Nikon Eclipse T5100 light microscope. n=3

Soft Agar Growth Analysis

In addition to growth on plastic, we examined the growth phenotype of KRAS Q61 mutants in soft agar to evaluate anchorage-independent growth, a hallmark of cancer cells.

Colonies of cells grown in soft agar were labeled and counted after 5 days. The results proved to be very similar with KRAS Q61E and Q61P having similar 3D growth as KRAS WT and EV. KRAS Q61H, Q61R, and Q61L were more similar to positive control KRAS G12D than negative control KRAS WT. In comparison to the light microscopy images, KRAS Q61L and KRAS Q61R showed an increase in Calcein uptake compared to KRAS G12D, suggesting that these mutations are more potentially transforming than the KRAS G12D control.

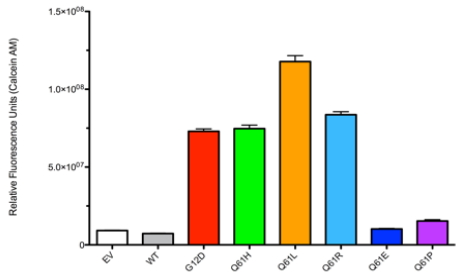

Figure 5. KRAS Q61 mutations do not cause equivalent transformation in 3D growth. Transformation trends match those from 2D assays. RIE-1 cells were infected with mutant KRAS and grown in soft agar. After 5 days, soft agar colonies were quantified after labeling with Calcein AM cell viability dye using a SpectraMax MiniMax. Error bars indicate standard error.

Determining Cell Signaling using Western Blotting

It would be expected that the KRAS-expressing cells that displayed greater morphological transformation had stronger activation of effector signaling that control cell growth, proliferation, and survival. To determine the levels of cell signaling and pathway activation that each KRAS Q61 mutant would induce, western blotting analysis was performed on KRAS-infected RIE-1 cells (Figure 6). We probed for activation of the ERK MAPK and PI3K-AKT pathways (Figure 3). We found that the KRAS Q61 mutants showed similar levels of activation through the MAPK pathway,

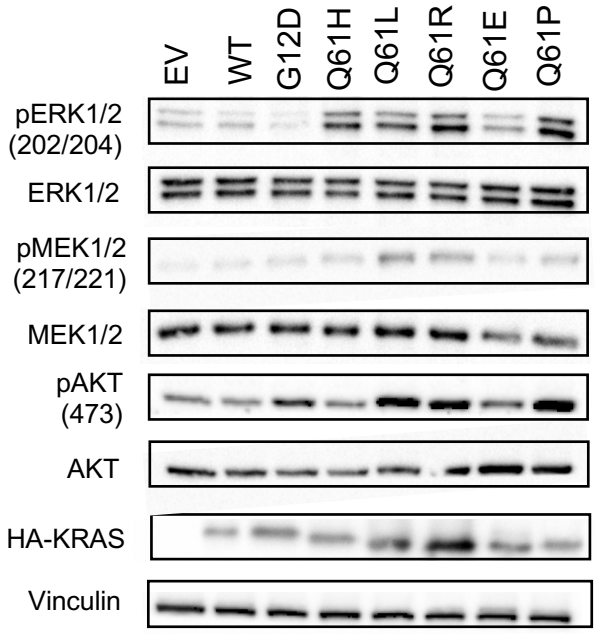

Figure 6. KRAS Q61 mutations do not equally activate RAS-mediated signaling pathways. Western blot analysis of RIE-1 cells expressing KRAS mutants was performed after 5 days of antibiotic selection with puromycin. (RIE-1, n>3)

despite differences seen in morphological transformation of NIH 3T3 cells. However, there were slight differences in pathway activation. Relative to the other mutations, KRAS Q61L exhibited a mild increase in phosphorylated and activated MEK1/2 (pMEK), and KRAS Q61R exhibited a mild increase in phosphorylated MEK1/2 (pMEK) and phosphorylated ERK1/2 (pERK). KRAS Q61E exhibited a mild decrease in MEK1/2, phosphorylated MEK1/2 (pMEK), and phosphorylated ERK (pERK). In the PI3K-AKT pathway, a similar trend was seen. However, Q61E and Q61H were much less active than the other mutants (Q61R, Q61L, Q61P) as indicated by a decrease in phosphorylated and activated AKT (pAKT).

Macropinocytosis Assays

To assess metabolic changes owed to KRAS mutation-specific effects, we performed macropinocytosis assays (Figure 7). Macropinocytosis is a vesicular process by which cancer cells acquire extracellular nutrients to support the increased energy needs of cancer cells. KRAS-transformed RIE-1 cells were serum starved to measure the uptake of a fluorescently labeled sugar from the growth medium (FITC-dextran). We found that the levels of

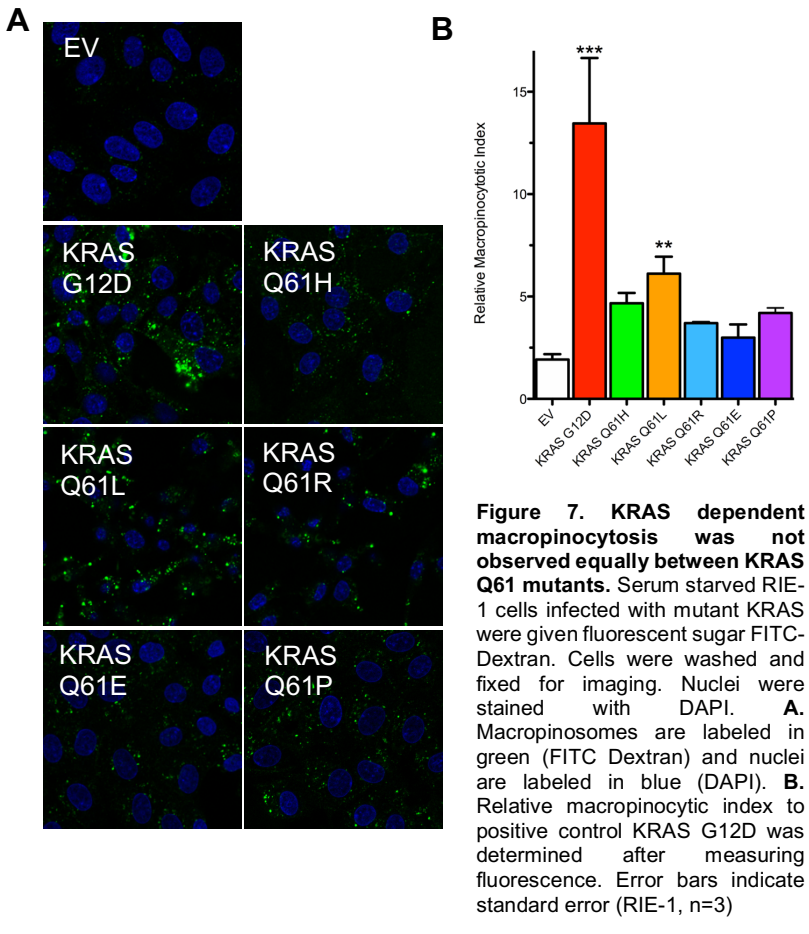

Figure 7. KRAS dependent macropinocytosis was not observed equally between KRAS Q61 mutants. Serum starved RIE-1 cells infected with mutant KRAS were given fluorescent sugar FITC-Dextran. Cells were washed and fixed for imaging. Nuclei were stained with DAPI. **A.** Macropinosomes are labeled in green (FITC Dextran) and nuclei are labeled in blue (DAPI). **B.** Relative macropinocytic index to positive control KRAS G12D was determined after measuring fluorescence. Error bars indicate standard error (RIE-1, n=3)

KRAS-dependent macropinocytosis differed greatly between the Q61 mutations. KRAS Q61H, Q61R, Q61E and Q61P had similar levels of micropinocytosis as EV, whereas KRAS Q61L was more similar to KRAS G12D. However, we also found that despite differences between each mutation, all Q61 mutants displayed significantly lower levels of macropinocytosis as compared to KRAS G12D. Further, the trends observed were not easily correlated with levels of signaling activity in our western blots.

Stress Fiber Formation Assays

To continue profiling our Q61 mutations in NIH 3T3 cells, we stained and profiled for actin stress fiber formation (actin) and focal adhesion formation (vinculin), processes that regulate cell shape and adhesion (Figure 8). It has been shown that expression of an activated KRAS mutant leads to suppression of actin stress fiber formation and focal adhesions, resulting in the classic "transformed" phenotype described earlier. Interestingly, Q61E was the only mutation that increased actin stress fiber formation as compared to EV (Figure 8A). Q61E also showed upregulation of focal adhesion assembly compared to EV (Figure 8B). The other Q61 mutations tested were more similar to the activating G12D mutation and showed suppression of this actin signature instead.

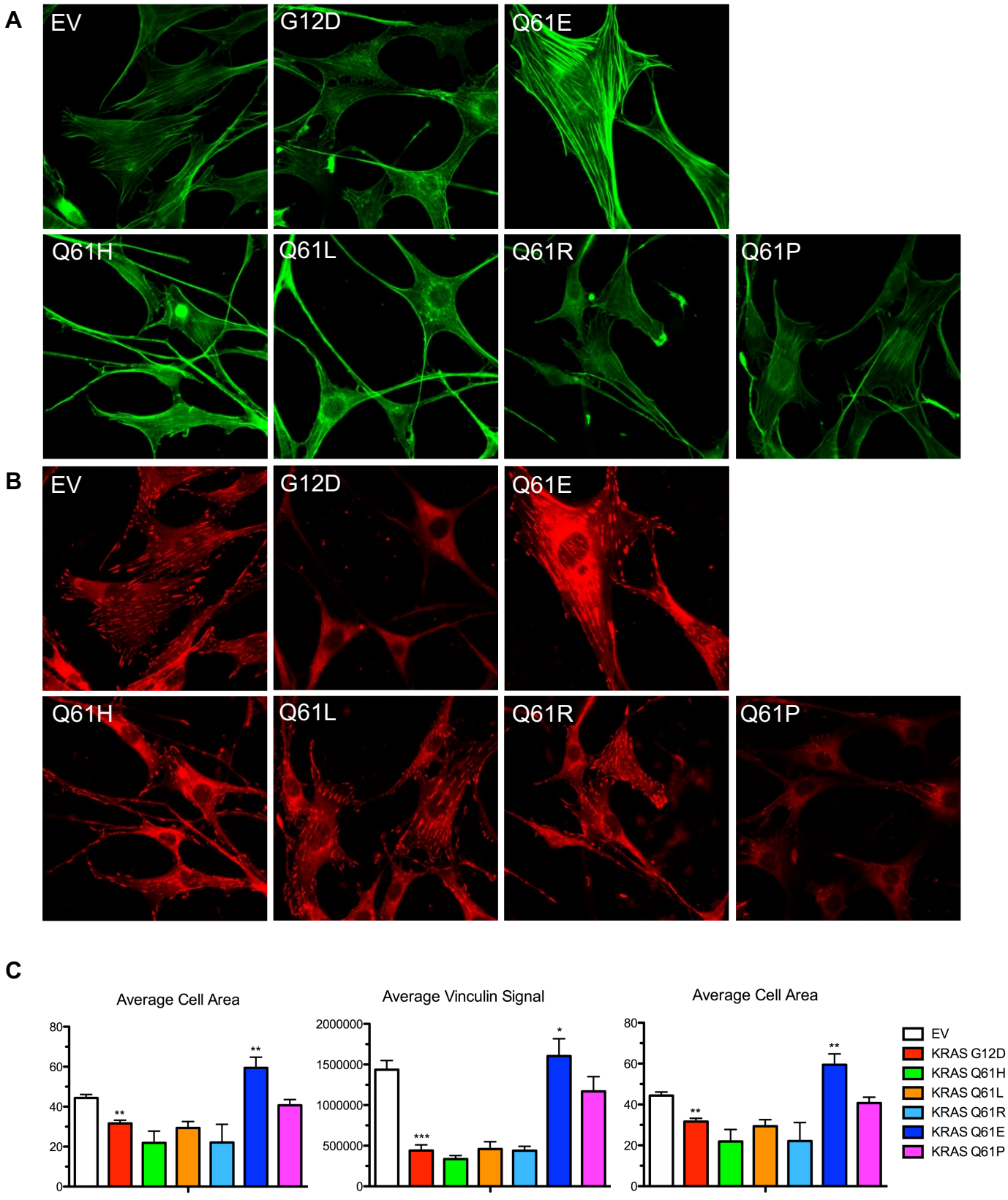

Figure 8. **KRAS Q61E promotes stress fiber formation**. NIH 3T3 cells expressing KRAS mutants were grown on fibronectin-coated slides and fixed for immunofluorescence labeling. Cells were stained and imaged on a Zeiss LSM 700 confocal microscope (63X). Cells were stained for (**A**) actin (n=3) and (**B**) vinculin (n=3). **C.** Average actin and vinculin signal presented as normalized to cell area. Error bars indicate standard error.

Random Cell Migration Assays

Upregulation of actin stress fiber formation may lead to reduced cell motility due to increased cellular adhesion. To test this, cell migration assays were performed to determine cell motility for each Q61 mutation (Figure 9). In NIH-3T3 cells, we found that KRAS Q61E migrated slower than the KRAS G12D control cells. The other Q61 mutations of interest (Q61H, Q61L, Q61R, Q61P) exhibited fairly similar amounts of cell migration, which was most similar with KRAS G12D.

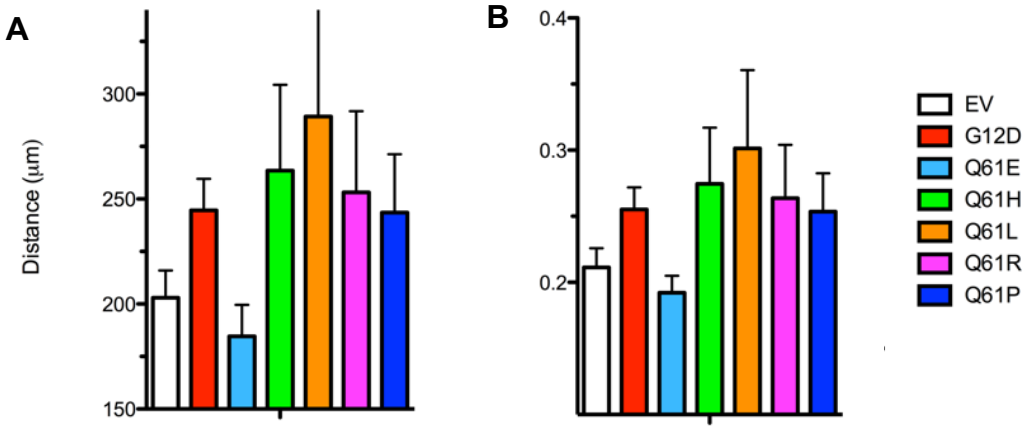

Figure 9. **KRAS Q61E mutation exhibits less cell migration compared to other mutations and EV.** NIH 3T3 cells were infected with mutant KRAS Q61 DNA and plated subconfluently on dishes coated in fibronectin. Dishes were imaged on Olympus VivaView Incubator Microscope at 10X for 12-16 hours. **A.** (distance) **and B.** (velocity) Cells were plated on 10 ug/mL fibronectin and individual cells were tracked for the course of 16 hours. Error bars indicate standard error. (n=3, N>60 cells per KRAS mutation)

RAS Nucleotide Exchange Assays

Based on the differing biological trends between the KRAS Q61 mutants, we expected there to be distinct alterations between the structures and functions of these mutant proteins that would result in these phenotypes. To determine functional differences due to specific KRAS Q61 mutations, we performed nucleotide exchange assays to determine both intrinsic and GEF-stimulated rates. We found that the intrinsic rates of nucleotide exchange of Q61L, Q61R, and Q61P were on a similar order of magnitude to that of WT KRAS (Figure 10). Q61R and Q61P had

slower nucleotide exchange rates than WT KRAS, whereas Q61L showed a faster exchange rate than shown in the literature [48].

RASGEF-mediated nucleotide exchange rates were determined by performing the assay in the presence of equimolar concentrations of the catalytic domain of SOS (a RASGEF) (Figure 10). The Q61E and Q61P mutants were similar with rates slower than the SOS-mediated nucleotide exchange of WT KRAS. The Q61R mutant had nucleotide exchange rates even slower than WT KRAS, Q61E, and Q61P. In fact, Q61R appeared to not be stimulated by GEF at all (Figure 10). Consistent with the increased intrinsic exchange rates, Q61L had a much faster rate of SOS-mediated nucleotide exchange compared to WT KRAS as well (Figure 10).

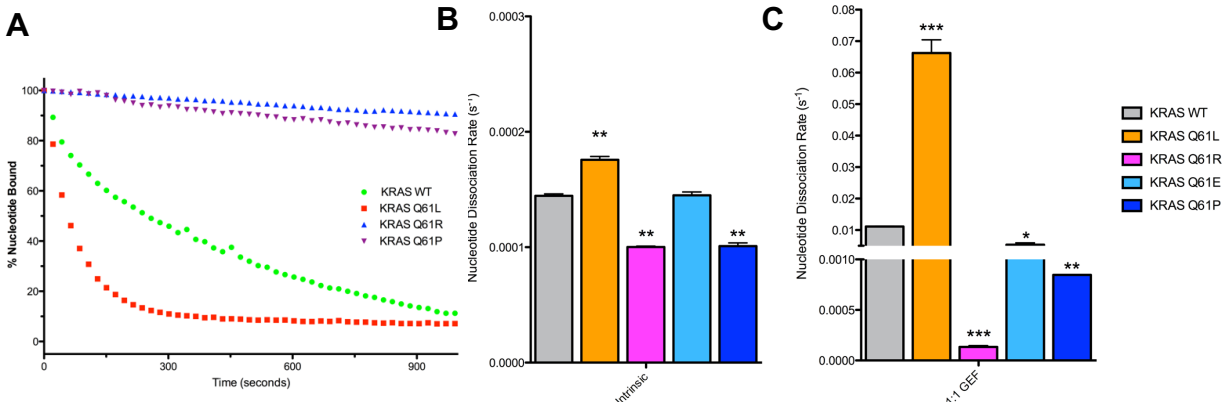

Figure 10. KRAS Q61 mutations have differing effects on nucleotide exchange. Purified KRAS protein was loaded with fluorescent nucleotide analog (mant-GTPγS). Agilent Cary Eclipse Fluorescence Spectrophotometer measured change in fluorescence after GDP was added without SOS (intrinsic) and in the presence of SOS (GEF-mediated). Change in fluorescence was used to find nucleotide exchange rate. **A.** Nucleotide exchange curves representative of experiment **B.** Q61R and Q61P show slower intrinsic nucleotide exchange rates compared to WT KRAS while Q61L exhibits a much faster rate of nucleotide exchange. **C.** KRAS Q61L shows increased GEF-mediated nucleotide exchange, while KRAS Q61R shows little stimulation. Error bars indicate standard error. (n=3)

Effector Binding Assays

To further characterize changes between the KRAS Q61 mutants, we performed RAS effector binding assays to determine the binding affinities of certain effector proteins. This analysis utilized recombinant proteins corresponding to the isolated RAS-binding (RBD) or RAS-association (RA) domains that bind preferentially to the active GTP-bound form of KRAS. Despite

significant decreases in binding in most cases, all Q61 mutations showed similar decreases in binding affinity for BRAF-RBD, CRAF-RBD, RALGDS-RA, and PLCe-RA compared to WT and KRAS G12D (Figure 11). Interestingly, KRAS Q61L had a significantly higher binding affinity for the RGL2-RA effector protein compared to the other mutations and WT KRAS (Figure 11).

A

	CRAF (RBD - nM)	RALGDS (RA - uM)	PLCε (RA - uM)
KRAS WT	61 ± 6	1.1 ± 0.1	0.72 ± 0.1
$KRAS^{G12D}$	664 ± 20	1.93 ± 0.3	0.77 ± 0.13
$KRAS^{Q61H}$	471 ± 24	8.82 ± 0.3	1.15 ± 0.21
$KRAS^{Q61L}$	605 ± 29	11.1 ± 0.3	1.81 ± 0.3
$KRAS^{Q61R}$	209 ± 14	8.07 ± 0.4	1.14 ± 0.1

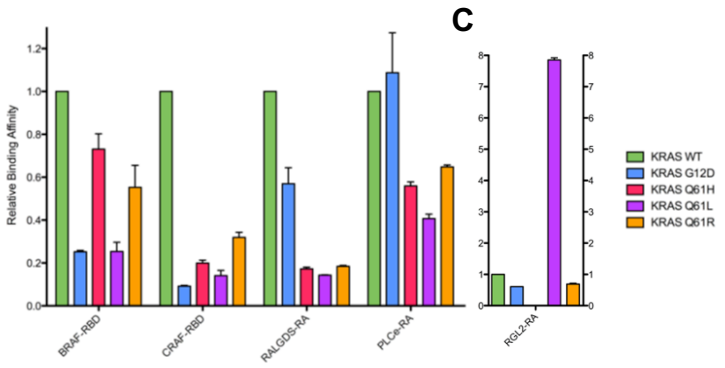

Figure 11. KRAS Q61 mutants showed altered binding to effector proteins. Purified KRAS proteins were loaded with the non-hydrolyzable nucleotide mant-GMPPNP and incubated with different concentrations of effector proteins. SpectraMax M5 plate reader measured change in fluorescence after GDP was added in excess. Changes in nucleotide exchange rates were plotted against protein concentrations to determine binding affinity. **A.** Determined binding constants of KRAS proteins to effector domains normalized to KRAS WT. **B.** Relative binding affinities as normalized to KRAS WT. KRAS proteins were preloaded with MANT-GMPPNP and nucleotide dissociation was measured in the presence of increasing concentrations of effector proteins to determine binding affinities. KRAS4B (2-169) proteins and effector fragments (CRAF-RBD, RALGDS-RA, PLCε- R) were expressed and purified from E. coli. See color legend to right. **C.** Relative binding affinities as normalized to KRAS WT. KRAS proteins were preloaded with MANT-GMPPNP and nucleotide dissociation was measured in the presence of increasing concentrations of effector protein RGL2-RA to determine binding affinities. See color legend to right.

Discussion

Based on our experimental results, the KRAS Q61 mutants we have tested are shown to be biochemically and biologically different as exhibited by alterations in cell morphology, cell signaling, KRAS-dependent macropinocytosis, stress fiber formation, cell migration, nucleotide exchange, and effector binding affinity.

Given that Q61 mutations are classically expected to activate RAS, the changes in morphology of NIH 3T3 cells upon KRAS infection were as expected with most of our Q61 mutations [35]. However, two mutations, Q61E and Q61P, did not appear to be potently activated mutant KRAS based on their ability to cause morphological changes, despite activating

effector signaling to similar levels. However, from our western blotting analyses, ERK-MAPK cell signaling appears to be consistently elevated across Q61 mutations (despite very small differences), suggesting a similarity among them. This discrepancy between morphological traits and pathway activation suggests a biological difference between Q61E/Q61P and other Q61 mutations beyond their activation of the primary signaling cascade. In addition to the ERK-MAPK pathway, there are at least 10 other known RAS effector families. These pathways could also show varying levels of activation from Q61 mutants, indicating more discrepancies between biological trends and pathway activation.

Interestingly, based on levels of activated MEK and ERK (as well as other signaling markers not shown), the Q61 mutations appear more potent in signaling than the G12D mutation in this pathway, suggesting a commonality to this mutation hotspot. However, the differences in the PI3K-AKT pathway prove that there are biological dissimilarities between Q61 mutants. All Q61 mutants exhibit similar activation except for Q61E and Q61H, which are less active in the PI3K-AKT pathway. The results from our analyses indicate there are functional differences among KRAS Q61 mutants given the varying trends. In order to identify a signaling basis for the different cancer causing potencies of the different Q61 mutants, we will interrogate additional cell signaling pathways and further experimentation specific to each mutation will be pursued.

There is much evidence that macropinocytosis, an endocytic process during which cells uptake extracellular macromolecules and fluid, is upregulated in cancer cells and is beneficial for cell proliferation by gaining more nutrients to grow [38]. Cancer cells have a very high metabolic demand, and macropinocytosis satisfies this demand to help the cells proliferate quickly [39]. Further, it has recently been shown that in KRAS-transformed cells, there is an upregulation of

macropinocytosis in which extracellular macromolecules are internalized via endocytosis as supplementary mechanism for metabolic needs. [38, 40-41] We performed macropinocytosis assays and found that Q61E, Q61P and Q61H expressing cells exhibit lower levels of macropinocytosis than the other Q61 mutants. KRAS Q61L undergoes more macropinocytosis and is more similar to KRAS G12D than the other mutations (Q61H, Q61R, Q61E, and Q61P were more to EV). However, all Q61 mutations showed lower basal macropinocytosis activities than the control KRAS G12D cell line. Interestingly, the Q61L mutation stands out here as the most potent mutation despite correlating well with the Q61H and Q61R mutations in aforementioned experiments.

The upregulation of actin stress fiber formation occurs in response to certain cell communication pathways [42]. For example, RHOA, another RAS family small GTPase, regulates formation of stress fibers and focal adhesions [43-45]. Previous literature has shown that expression of activated KRAS mutations suppress RHOA signaling and stress fiber formation [46] Interestingly, the Q61E mutation appears to have more upregulated stress fiber formation than EV. The mutation also resulted in an increase in focal adhesions which serve as biochemical signaling linkages for cellular adhesion. This is further emphasized by the fact that all other Q61 mutations resulted in suppression of this stress fiber phenotype similar to the G12D mutation. This could indicate that Q61E promotes different pathways than the other Q61 mutations to control growth, possibly through upregulation of RHOA signaling pathways [36].

Higher levels of stress fiber formation should lead to decreased cell motility due to increased attachment and contractility of the cells. The decreased migration distance and speed of the KRAS Q61E mutation is therefore not surprising based on the higher levels of actin stress

fiber formation. We would expect that KRAS Q61E is not as metastatically invasive as the control KRAS G12D or other Q61 mutants based on these experiments in vitro, which may be a phenotype that contributes to its lower transforming capabilities.

To complement our biological studies, we also performed biochemistry assays to further characterize these mutations, as alterations in biochemical and structural properties may support potential mechanisms for the differences in morphology, cell signaling, and other biological phenotypes we observe. As the Q61 mutation is located in the RAS Switch 2 region (KRAS residues 59-67) by the SOS-binding site of KRAS proteins, structural differences among the proteins could contribute to varying binding affinities for the RASGEF, SOS, which could also result in biochemical and biological discrepancies among the mutations [47].

Additionally, the different side chains for each mutation also result in different intrinsic nucleotide exchange rates as Switch 2 plays a role in nucleotide binding. Q61L's faster rate of GEF-mediated nucleotide exchange indicates it is more sensitive to SOS than the other mutations (Q61R and Q61P), which could be attributed to the differences in its binding affinity for this RASGEF. As SOS has two RAS binding sites (a catalytic domain and an allosteric site responsible for accelerating exchange rates further) it is possible that the affinity of the Q61L mutant for the allosteric binding site of SOS is increased [47]. This would allow it to speed up the protein's nucleotide exchange compared to other mutations. The hydrophobic side chain of Q61L could structurally alter the SOS binding site so that its binding affinity for this RASGEF is greater than WT, Q61R, and Q61P. On the other hand, the rigidity of Q61P could alter the protein so that it decreases the protein's binding affinity for SOS resulting in slower nucleotide exchange rates.

Interestingly, the molar polar side chain substitution of Q61R results in little-to-no stimulation by SOS at all, suggesting a deficiency for binding to the GEF altogether.

In addition to GEFs and GAPs, RAS proteins also bind to effector proteins to regulate different cell signal transduction pathways [33-34]. Based on the differences in biology seen, we expect that different Q61 mutations will show differential binding to effector proteins. Most of the Q61 mutations we tested appear to have a lower binding affinity for effector proteins than KRAS WT, but also do not greatly differ from each other. Therefore, these altered affinities are not significant enough to explain some of the differential signaling effects we observe.

However, the increased affinity of Q61L for RGL2-RA indicates this mutation may activate this effector more than WT KRAS. Q61L may have elevated activation of RAL-mediated signaling through RGL2-RA, suggesting that targeting this pathway may be a potential avenue for inhibiting this mutant. However, this increase in binding affinity may not be high enough to significantly alter growth phenotypes. It would be important to validate the contribution of this effector protein as well as how other effector proteins may differ in compensation.

After experimental analysis, it was determined that biological and biochemical differences do exist between the KRAS Q61 mutants. Our results show that mutation-specific vulnerabilities may offer new targets for therapy development. However, additional experimentation in vitro and in vivo must be performed to determine the true physiological significance of these differences.

Acknowledgements

I would like to thank the members of the Der Lab, especially my mentor, Minh Huynh, and the principal investigator, Dr. Channing Der, for their help and support during my undergraduate research career. Our funding came from the NIH NCI, Pancreatic Cancer Action Network, and CDMRP. I would also like to thank my readers, Dr. Steve Matson and Dr. Scott Williams, my writing group, and my thesis class professor, Dr. Amy Maddox, for their help and support this semester during the finalization of my thesis paper and presentation.

References

1. Cox, A. D., Fesik, S. W., Kimmelman, A. C., Luo, J. & Der, C. J. Drugging the undruggable RAS: Mission Possible? Nature Reviews Drug Discovery 13, 828–851 (2014).
2. Fernández-Medarde, A., Santos, E., Ras in Cancer and Developmental Diseases. Genes Cancer. 3, 344-358 (2011).
3. Rojas, J. M., Santos, E., Ras Genes and Human Cancer: Different Implications and Different Roles. Current Genomics 3, 295-311 (2002).
4. Karnoub, A.E., Weinberg, R. A., Ras oncogenes: split personalities. Nature Reviews Molecular Cell Biology. 7, 517-531 (2008)
5. Papke, B. & Der, C. J. Drugging RAS: Know the enemy. Science 355, 1158–1163 (2017).
6. Siegel, R. L., Miller, K. D. and Jemal, A. (2017), Cancer statistics, 2017. CA: A Cancer Journal for Clinicians, 67: 7–30. doi:10.3322/caac.21387
7. American Cancer Society. Cancer Facts & Figures 2017. Atlanta: American Cancer Society; 2017.

8. Pasca di Magliano, M., Logsdon, C. D., Roles for KRAS in Pancreatic Tumor Development and Progression. Gastroengerology 6, 1220-1229 (2013).
9. Jones, S., Zhang, X., et al., Core Signaling Pathways in Human Pancreatic Cancers Revealed by Global Genomic Analyses. Science 321, 1801-1806 (2008)
10. N. Waddell, et al. Whole genomes redefine the mutational landscape of pancreatic cancer. Nature. 518, 495-501) (2015)
11. Reuther, G. W., Der, C. J. The Ras branch of small GTPases: Ras family members don't fall far from the tree. Current Opinion in Cell Biology. 12, 157-165 (2000)
12. Chakrabarti, M., Jang, H., Nussinov, R. Comparison of the Conformations of KRAS Isoforms, K-Ras4A and K-Ras4B, Points to Similarities and Significant Differences. J Phys Chem B 4, 667-679 (2016)
13. Zhou, B., Der, C.J., Cox, A.D. The role of wild type RAS isoforms in cancer. Semin Cell Dev Biol. 58, 60-69 (2016)
14. Castellano, E., Santos, E. Functional Specificity of Ras Isoforms. Genes Cancer. 3, 216-231 (2011)
15. Abankwa, D., Gorfe, A. A., Hancock, J. F., Mechanisms of Ras membrane organization and signaling. Cell Cycle. 17, 2667-2673 (2008)
16. Newlaczyl, A. U., Hood, F.E., et. al. Decoding RAS isoform and codon-specific signaling. Biochem Society Transactions. 4, 742-746 (2014)
17. Prior IA, Hancock JF. Ras trafficking, localization and compartmentalized signaling. Seminars in cell & developmental biology. 2, 145–153 (2012)

18. Hancock, J., Parton, R. G. Ras plasma membrane signaling platforms. Biochem J. 389, 1-11 (2005)
19. Bourne, H.R., Sanders, D.A, McCormick, F. The GTPase superfamily : a conserved switch for diverse cell functions. Nature. 348, 125-132 (1990)
20. Hobbs, G. A., Der, C. J. & Rossman, K. L. RAS isoforms and mutations in cancer at a glance. Journal of Cell Science 129, 1287–1292 (2016).
21. Bos, J. L., Rehmann, H. & Wittinghofer, A. GEFs and GAPs: critical elements in the control of small G proteins. Cell 129, 865–877 (2007).
22. Scheffzek, K., Ahmadian M.R., The Ras-RasGAP complex: structural basis for GTPase activation and its loss in oncogenic Ras mutants. Science. 277, 333-338 (1997).
23. Gideon, P., John, J., Frech, M., et. al. Mutational and kinetic analyses of the GTPase-activating protein (GAP)-p21 interaction: the C-terminal domain of GAP is not sufficient for full activity. Molecular and Cellular Biology. 12, 2050-2056 (1992)
24. Li, G., Zhang, X.C. GTP Hydrolysis mechanism of Ras-like GTPases. J Mol Biol. 5, 921-932 (2004)
25. Hanahan, D., Weinberg, R. A. Hallmarks of cancer: the next generation. Cell. 5, 646-674 (2011)
26. Bos, J. L., The ras gene family and human carcinogenesis. Mutation Research 195, 255-271 (1988)
27. Campbell, S.L., Khosravi-Far, R., Rossman, K.L., Der, C.J., Increasing complexity of Ras signaling. Oncogene 17, 1395-1413 (1998).
28. Bos J. L. ras oncogenes in human cancer: a review. Cancer Res. 49:4682–4689 (1989)

29. Bar-Sagi, D. A Ras by Any Other Name. Molecular Cell Biology. 5, 1441-1443 (2001)
30. Hancock, J.F., Ras proteins: different signals from different locations. Nature Reviews Molecular Cell Biology. 4, 373-385 (2003)
31. RAS mutation frequencies compiled using Catalogue of Somatic Mutations in Cancer (COSMIC) v86
32. Fotiadou, P.P., Takahashie, C., Wild-Type NRas and KRas Perform Distinct Functions During Transformation. Molecular and Cellular Biology. 27, 6742-6755 (2007)
33. Bivona, T. G., Philips, M.R. Ras pathway signaling on endosomembranes. Current Opinion in Cell Biology. 15, 136-142 (2003)
34. Khosravi-Far, R., Solska, P. A., et. al. Activation of Rac1, RhoA, and Mitogen-Activated Protein Kinases is Required for Ras Transformation. Molecular and Cell Biology. 15, 6443-6453 (1995)
35. Lu, S., Jang, H., Nussinov, et. al., The structural basis of Oncogenic Mutations G12, G13, and Q61 in small GTPase K-Ras4B. Scientific Reports 6 21949 (2016)
36. Stafford, A. J., Walker, D. M., Webb, L. J., Electrostatic Effects of Mutations of Ras Glutamine 61 Measured Using Vibrational Spectroscopy of a Thiocyanate Probe. Biochemistry. 51, 2757-2767 (2012)
37. Burhman, G., Holzapfel, G., Allosteric modulation of Ras positions Q61 for a direct role in catalysis. Proceedings of the National Academy of Sciences of the United States of America 107, 4931-4936 (2010)
38. Jing, L., Wang, J., et. al. The greedy nature of mutant RAS: a boon for drug discovery targeting cancer metabolism? Acta Biochimica et Biophysica Sinica. 48, 17-26 (2015)

39. Trajkovska, M. Macropinocytosis supports cancer cell proliferation. Nature Cell Biology, 15, 729. (2013).
40. Commisso, C. et al. Macropinocytosis of protein is an amino acid supply route in Ras-transformed cells. Nature 497, 633–637 (2013).
41. Machesky, L. M., Hall, A. Role of actin polymerization and adhesion to extracellular matrix in Rac- and Rho- induced cytoskeletal reorganization. J Cell Biology. 4, 913-926 (1997)
42. Sahai, E., Olson, M. F., Marshall, C. J. Cross-talk between Ras and Rho signaling pathways in transformation favors proliferation and increased motility. EMBO Journal. 4, 755-766 (2001)
43. Biancur, D. E., Kimmelman, A. C. The plasticity of pancreatic cancer metabolism in tumor progression and therapeutic resistance. Biochimica et Biphysica Acta – Reviews on Cancer. 1870, 67-75 (2018)
44. Ridley, A.J., Hall, A. The small GTP-binding protein rho regulates the assembly of focal adhesions and stress fibers in response to growth factors. Cell, 3, 389-399 (1992)
45. Amano, M. Chihara, K., et. al. Formation of actin stress fibers and focal adhesions enhanced by Rho-kinase. Science, 275, 1308-1311 (1997).
46. Khosravi-Far, R., et. al. Dbl and Vav mediate transformation via mitogen-activated protein kinase pathways that are distinct from those activated by oncogenic Ras. Molecular and Cellular Biology, 14, 6848-6857 (1994).
47. Margarit, S. M. Sondermann, H., et. al. Structural evidence for feedback activation by Ras.GTP of the Ras-specific nucleotide exchange factor SOS. Cell, 5, 685-695 (2003).

48. Smith, M., et. al. NMR-based functional profiling of RASopathies and oncogenic RAS mutaitons. PNAS, 110, 4574-4579 (2013).